Title	Specimen- and grain-size dependence of compression deformation behavior in nanocrystalline copper
Author(s)	Okamoto, Norihiko L.; Kashioka, Daisuke; Hirato, Tetsuji; Inui, Haruyuki
Citation	International Journal of Plasticity (2014), 56: 173-183
Issue Date	2014-05
URL	http://hdl.handle.net/2433/187145
Right	© 2013 Elsevier Ltd.
Type	Journal Article
Textversion	author

Specimen- and Grain-Size Dependence of Compression Deformation Behavior in Nanocrystalline Copper

by Norihiko L. Okamoto[1,2,*], Daisuke Kashioka[1], Tetsuji Hirato[3] and Haruyuki Inui[1,2]

[1]*Department of Materials Science and Engineering, Kyoto University, Kyoto 606-8501, Japan*
[2]*Center for Elements Strategy Initiative for Structure Materials (ESISM), Kyoto University, Sakyo, Kyoto 606-8501, Japan*
[3]*Graduate School of Energy Science, Kyoto University, Sakyo, Kyoto 606-8501, Japan*

***Corresponding Author Contact Information:**
Norihiko L. Okamoto
Department of Materials Science and Engineering, Kyoto University
Sakyo-ku, Kyoto 606-8501, Japan
Tel: +81-75-753-5481, Fax: +81-75-753-5461
E-mail: okamoto.norihiko.7z@kyoto-u.ac.jp

Abstract

The compression deformation behavior of electrodeposited nanocrystalline copper pillars with average grain sizes (d) of 360, 100, and 34 nm has been investigated as a function of specimen size (D). The yield stress for nanocrystalline pillars with d = 360 and 100 nm does not depend on specimen size, exhibiting essentially the bulk yield stress until the specimen size is reduced down to the critical values ((D/d)* = 35 and 85), below which the yield stress decreases with the decrease in specimen size. In contrast, the yield stress for nanocrystalline pillars with d = 34 nm does not depend much on specimen size, exhibiting the bulk yield stress value for all specimen sizes investigated. The dominant deformation mechanism changes from dislocation glide for pillars with d = 360 and 100 nm to grain boundary

diffusional creep for pillars with d = 34 nm. Grain-size induced softening occurs for pillars with d = 34 nm being consistent with the occurrence of change in deformation mechanisms, whereas the bulk yield stress for pillars with d = 360 and 100 nm increases with the decrease in grain size according to the classical Hall−Petch relationship. The critical $(D/d)^*$ values determined for nanocrystalline Cu pillars with d = 360 and 100 nm increases with the decrease in grain size so as to conform to the same power law scaling obtained for coarse-grained Cu polycrystals. This is the first indication that the specimen size-induced softening extends from micrometer to nanometer scales as far as the dominant deformation mechanism is dislocation glide. The considerably large critical $(D/d)^*$ values determined for nanocrystalline Cu pillars with d = 360 and 100 nm are discussed in terms of strain continuity among neighboring grains and the generation of geometrically necessary dislocations to maintain strain continuity at the grain boundaries.

Keywords: Dislocations (A); Crystal plasticity (B); Polycrystalline material (B); Mechanical testing (C); Focused ion beam (FIB) method.

1. Introduction

The control of materials properties is usually made by manipulating materials length scales such as grain size and sample size. Grain refinement is a usual practice in improving strength of materials. In coarse-grained polycrystalline metals, plastic deformation occurs via the glide of lattice dislocations and their interaction with grain boundaries (GBs). Since GBs are obstacles to the initiation of bulk yielding and the subsequent propagation of plastic flow, the yield strength of material increases with the decrease in grain size, according to the well-known Hall−Petch relationship (Hall, 1951; Petch, 1953). Although there have been a few reports on nano-indentation hardness measurements in which the Hall−Petch relationship still holds true at a grain size of 10 nm (Chen et al., 2006; Knapp and Follstaedt, 2004), the Hall−Petch relationship usually breaks down and the yield strength of material tends to decrease with the decrease in grain size when the grain size is reduced to below 10−50 nm, leading to the emergence of the so-called “inverse Hall−Petch regime” (Chokshi et al., 1989; Detor and Schuh, 2007; Sanders et al., 1997; Schuh et al., 2003; Schuh et al., 2002; Trelewicz and Schuh, 2007, 2008). This has been attributed to the emergence of GB-mediated deformation such as GB sliding (Van Swygenhoven and Derlet, 2001), GB migration (Gianola et al., 2006; Legros et al., 2008; Rupert et al., 2009) and grain rotation (Shan et al., 2004; Wang et al., 2008) at these small grain sizes.

While these grain size effects are observed in bulk specimens where the sample

dimension is sufficiently large, sample size effect, another type of size effect, has recently attracted considerable attention not only for the importance in the medical and microelectronics industries but also for fundamental understanding of the underlying deformation mechanisms. When the sample size is decreased, the strength of single-crystal pillar samples with the size of tens of micrometers or less has been known to increase according to the power law scaling with the power exponent values not significantly varying from material to material for fcc (face-centered cubic) single crystals (Greer and De Hosson, 2011; Kraft et al., 2010; Uchic et al., 2009). This behavior has been frequently termed a "smaller is stronger" trend. However, the opposite (smaller is weaker) trend has long been known to occur for coarse-grained polycrystalline metals when the sample size is reduced so that the number of grains contained across the sample cross-section is significantly small (Armstrong, 1961; Hug and Keller, 2010; Janssen et al., 2006; Keller et al., 2011; Miyazaki et al., 1979; Pell-Walpole, 1943; Thompson, 1974). For many different fcc metals and alloys with the average grain sizes ranging from tens to hundreds of micrometers, the flow (yield) stress is reported to decrease with the decrease in sample size when the ratio (t/d) of sample size (thickness of the plate specimen (t) to average grain size (d)) is smaller than a critical value. The critical values, ((t/d)*), are reported to be in the range of 3−15, depending on grain size and stacking fault energy (Armstrong, 1961; Hug and Keller, 2010; Janssen et al., 2006; Keller et al., 2011; Miyazaki et al., 1979; Pell-Walpole, 1943; Thompson, 1974). For Cu, the

critical (t/d)* value is reported to increase from 5 to 13 when the grain size decreases from 140 to 16 μm (Miyazaki et al., 1979).

Then, a question arises as to how the mechanical properties vary with specimen size when the grain size is reduced considerably to the nanometer size range so that the glide of lattice dislocations is no longer the dominant deformation mechanism. This question arises from the expectation that two different size effects, grain size (intrinsic) and sample size (extrinsic) effects, may couple with each other in pillar compression tests of nanometer-sized polycrystalline metals. The results recently reported on this are indeed controversial. Jang and Greer (Jang and Greer, 2011) have observed a "smaller is weaker" trend in 60 nm-grained Ni polycrystals in pillar compression/tensile tests and found the sample size dependent weakening occurring at the (D/d)* value in the range of 15−30 where D is the pillar diameter. Gu et al. (Gu et al., 2012) have also observed a similar "smaller is weaker" trend in 12 nm-grained Pt polycrystals in pillar compression tests with the (D/d)* value in the range of 5−10. In contrast, Warthi et al. (Warthi et al., 2013) and Chen et al. (Chen and Ngan, 2011) observed an opposite 'smaller is stronger' trend in Ni nanowires and Ag microwires, respectively. Each of these studies was made with polycrystalline samples only with a fixed grain size, and nothing is known about how the softening (or strengthening) behavior is affected by the grain size and how the critical (D/d)* value varies with the grain size, as known for many fcc metals and alloys with the average grain sizes ranging from tens to

hundreds of micrometers (Armstrong, 1961; Hug and Keller, 2010; Janssen et al., 2006; Keller et al., 2011; Miyazaki et al., 1979; Pell-Walpole, 1943; Thompson, 1974).

In the present study, we investigate the compression deformation behavior of pillar specimens made from electrodeposited nanocrystalline Cu with three different average grain sizes ranging from 34 to 360 nm, in order to better understand the softening (or strengthening) behavior as a function of sample size and the ratio (D/d) of sample size (D) to average grain size (d).

2. Experimental methods

Nanocrystalline Cu films with a thickness of about 300 μm were prepared by pulsed electrodeposition in a plating bath composed of 0.72 mol/L copper sulfate ($CuSO_4$-$5H_2O$), 1.3 mol/L sulfuric acid (H_2SO_4), 5 mg/L gelatin and 0−67 mg/L thiourea (CH_4N_2S) with strips of stainless steel and Cu (3N purity) used respectively as the cathode and anode. The pulse width used was 1 second with the peak current density of 0.160 A cm^{-2} followed by a pause of 1 second. Gelatin was added in order to maintain the flatness of the deposition surface while thiourea to hinder the growth of deposited grains. Three different concentrations of thiourea (0, 1.2, and 67 mg/L) were chosen to control the grain size of Cu films. A fresh plating bath was used for each electrodeposition.

Deposited Cu films were sectioned, mechanically polished with SiC paper and then

electropolished at 12 V in a solution of nitric acid and methanol (3:7 by volume) at −40°C. Microstructures of deposited films were examined by a JEOL JSM−7001FA scanning electron microscope (SEM) equipped with an energy dispersive spectroscopy (EDS) apparatus and by a JEOL JEM−2000FX transmission electron microscope (TEM) operated at 200 kV. Specimens for TEM observations were prepared by electropolishing with a Struers Tenupol−3 twin-jet electropolisher, followed by ion-milling with 2 keV Ar ions. X-ray diffraction (XRD) was also carried out on the bottom (cathode) side of electrodeposited films with a Rigaku MiniFlex−II operated at 30 kV and 15 mA.

Pillar specimens with a square cross-section having the side length (D) ranging from 1.0 to 20.3 μm and an aspect ratio of 1:3 were machined from electropolished Cu films by using a JEOL JIB−4000 focused ion beam (FIB) apparatus at an operating voltage of 30 kV and a beam current of 100−300 pA. The strengthening effect due to the irradiation damage of high-voltage Ga^+ ions during FIB fabrication is considered to be negligible (Greer and Nix, 2006; Greer et al., 2005; Machalett et al., 2000). Uniaxial compression tests were conducted at room temperature at a constant stress rate of 1−3 MPa/s corresponding to a nominal strain rate of 3×10^{-5}−3×10^{-4} s^{-1} in the elastic region, with the use of a Shimadzu MCT-211 micro compression tester equipped with a flat punch indenter tip. Deformation microstructures were examined by SEM and scanning transmission electron microscopy (STEM) with the use of a JEOL JEM−2100F STEM operated at 200 kV. Specimens for STEM observations were

prepared by FIB cutting a slice from deformed specimen at 45° from the compression axis. Slices were mounted on a lacey carbon TEM grid by electrostatically picking-up with a glass filament (lift-out method) (Overwijk et al., 1993).

3. Results

3.1. As-electrodeposited microstructures

Cross-sectional SEM observations of as-electrodeposited films confirm the microstructural homogeneity across the film and the absence of porosities and microcracks regardless of deposition condition. Although sulfur incorporation is expected due to thiourea additions in the electrolytic bath, the sulfur concentration in the films are below the detection limit of SEM-EDS analysis. Bright-field TEM images of Cu films electrodeposited with the thiourea concentrations of 0, 1.2, and 67 mg/L are shown in Figs. 1(a)-(c), respectively. Most crystal grains are equiaxed regardless of the thiourea concentration, and the grain size decreases with the increase in the thiourea concentration. Growth twins (some of them may be simply stacking faults) with an approximate density of 2×10^3 m^2/m^3 are seen in many grains, but dislocations are hardly observed because partly of the difficulty in adjusting the diffraction conditions for each of nanometer-sized grains. The corresponding selected-area electron diffraction (SAED) patterns taken from an area approximately 3 μm in diameter are shown in Figs. 1(d)-(f), respectively. Positions of several Debye-Scherrer rings for pure fcc

Cu, CuO, Cu_2O, and CuS (Villars, 1997) are indicated in the figure. The appearance of Debye-Scherrer rings changes from 'continuous' in Fig. 1(f) to 'spotty' in Fig. 1(d), reflecting the increase in the grain size. Although most Debye-Scherrer rings are indexed as those from Cu, a faint ring is observed as the smallest radius ring (arrowed in Figs. 1(d)-(f)), which can be indexed as that from Cu_2O. The presence of the Debye-Scherrer ring of Cu_2O is due most probably to the surface oxidation of the TEM specimens, since dark-field TEM imaging formed by setting the objective aperture at a position on the faint ring does not indicate any particular localized areas responsible for the Debye-Scherrer ring and the intensity of the faint Debye-Scherrer ring tends to decrease when observed immediately after ion-polishing TEM specimen. There are no Debye-Scherrer rings that can be attributed to the presence of CuS.

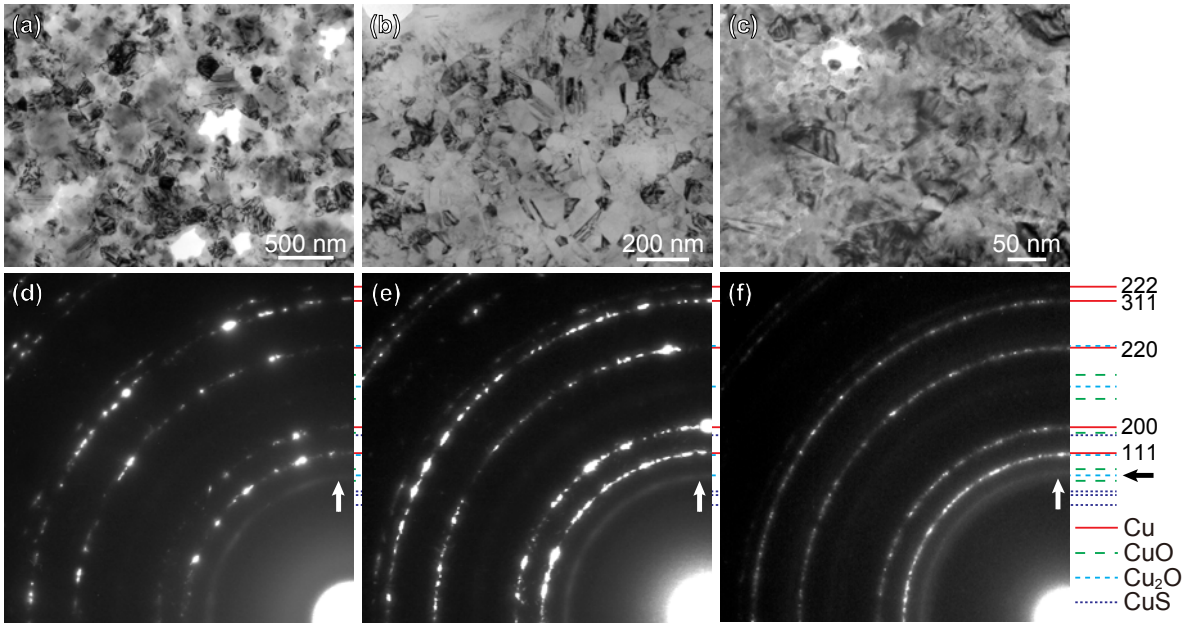

Fig. 1. (a-c) Bright-field TEM images, and (d-f) selected area diffraction patterns for the nanocrystalline Cu electrodeposited with the thiourea concentration of (a,d) 0, (b,e) 1.2, and (c,f) 67 mg/L, respectively.

The distribution of grain size is depicted in Figs. 2(a)-(c) respectively for Cu films electrodeposited with the thiourea concentrations of 0, 1.2, and 67 mg/L. Grain size measurements were made by the modified interception method (Arioka et al., 2001) with dark-field TEM images formed by setting the objective aperture at a position on the 111 Debye-Scherrer ring of Cu. Each of the grain size distributions in Figs. 2(a)-(c) can be fitted with a lognormal distribution function with the arithmetic mean grain size and standard deviation of 360 nm and 0.60 (Fig. 2(a)), 100 nm and 0.50 (Fig. 2(b)), and 34 nm and 0.66 (Fig. 2(c)), respectively. Electrodeposited films with the thiourea concentrations of 0, 1.2, and 67 mg/L are hereafter called according to their average grain sizes as those with the average grain size (d) of 360, 100, and 34 nm throughout this paper.

XRD patterns obtained from electrodeposited Cu films with the average grain size of 360, 100, and 34 nm are shown in Fig. 3, together with those calculated for randomly-oriented

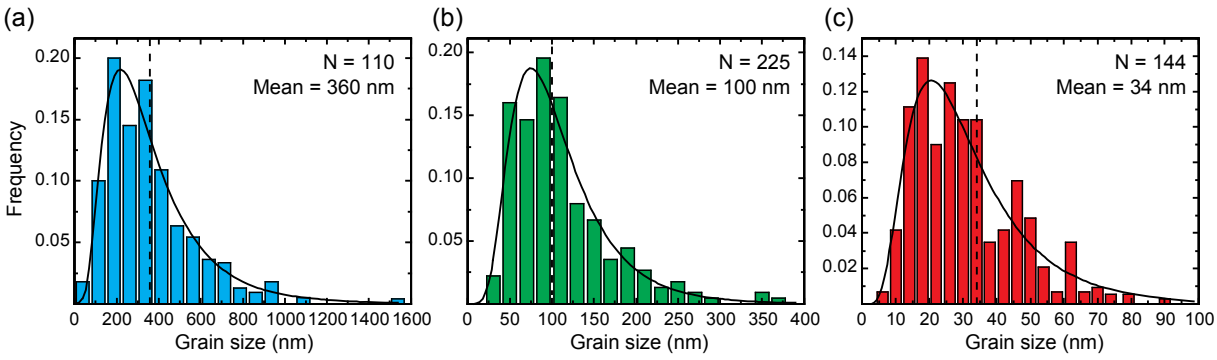

Fig. 2. Grain size distributions for the nanocrystalline Cu electrodeposited with the thiourea concentration of (a) 0, (b) 1.2, and (c) 67 mg/L, respectively. The curves and dotted lines are lognormal regression curves and arithmetic mean grain sizes, respectively.

Cu, CuO, Cu_2O and CuS. No XRD peaks other than those indexed as fcc Cu are observed, confirming that the presence of Cu_2O noted in the SAED patterns in Figs. 1(d)-(f) is indeed due to the surface oxidation of the TEM specimens. All XRD peaks indexed as fcc Cu are broadened as the average grain size decreases, with the extent of broadening being almost qualitatively consistent with the grain size reduction. Intensities of XRD peaks from fcc Cu are almost consistent with those calculated for a random orientation of grains, indicating the absence of any texture and preferred orientation for as-electrodeposited Cu films.

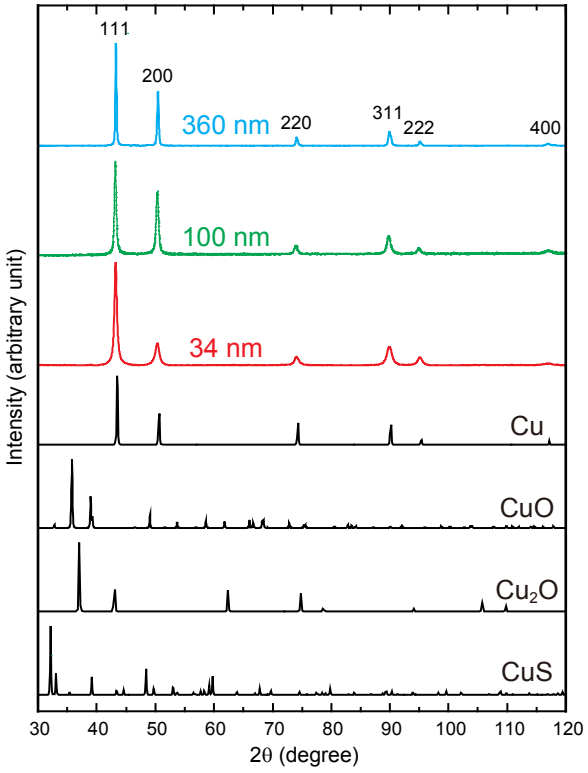

Fig. 3. XRD patterns obtained for electrodeposited copper films with average grain size of 360, 100, and 34nm. Calculated patterns for randomly oriented fcc copper, CuO, Cu_2O and CuS are also shown below the experimental ones.

3.2. Micropillar compression deformation behavior

Selected stress−strain curves obtained from micropillar specimens fabricated from electrodeposited films with d = 360, 100 and 34 nm are shown respectively in Figs. 4(a)-(c) for some different pillar specimen sizes (D). Stress−strain curves are smooth, exhibiting yielding followed by work-hardening without any discontinuity. Values of yield stress deduced as the 0.2% off-set flow stress by assuming the linear part in the stress−strain curves as the elastic deformation region for micropillar specimens with d = 360, 100 and 34 nm are plotted respectively in Figs. 4(d)-(f) as a function of specimen size. For pillars with d = 360 and 100 nm, the yield stress does not depend on specimen size exhibiting essentially the same values as their respective bulk (millimeter-sized) specimen when the specimen size is large. When the specimen size is small, however, the yield stress significantly decreases as the specimen size is decreased, clearly exhibiting the 'smaller is weaker' trend, as observed in nanocrystalline Ni (Jang and Greer, 2011) and Pt (Gu et al., 2012). The decrease in yield stress with the decrease in the specimen size is significantly large; the yield stress values obtained for the smallest specimen size is as small as about one forth that for their bulk values (75 % reduction) for both pillar with d = 360 and 100 nm. The specimen size below which the yield stress starts to decrease depends on the grain size. These critical specimen sizes are 12.5 and 8.5 μm for pillars with d = 360 and 100 nm, respectively. These correspond respectively to the critical (D/d) values, (D/d)*, of 35 and 85, both of which are considerably larger than

not only those determined for micrometer-sized Cu (5-13 for d = 16−140 μm (Miyazaki et al., 1979) and 2 for d = 2−24 μm (Yang et al., 2012)) but also those determined for 60 nm-grained Ni (15−30) (Jang and Greer, 2011) and 12 nm-grained Pt (5−10) (Gu et al., 2012). For pillars with d = 34 nm, on the other hand, the yield stress does not depend much on specimen size, exhibiting the bulk yield stress value for all specimen sizes investigated (at least, up to D=0.4 mm; D/d~12). The value of bulk yield stress for pillars with d = 34 nm is smaller than those for pillars with d = 360 and 100 nm, indicating the occurrence of grain-size induced softening. This is in agreement with the results by Chokshi et al. (Chokshi et al., 1989) that grain size-induced softening occurs below 50 nm for Cu.

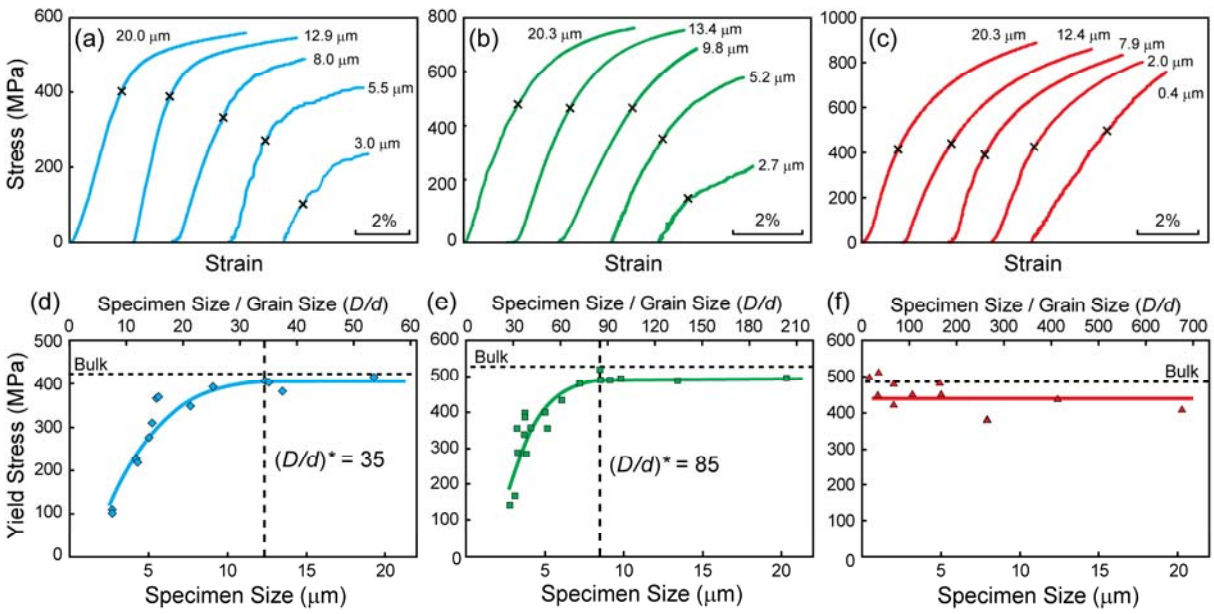

Fig. 4. Representative compression stress−strain curves for pillars of various sizes fabricated from the electrodeposited films with d = (a) 360, (b) 100, and (c) 34 nm, respectively. Values of yield stress plotted as a function of the specimen size (side length, D) for d = (d) 360, (e) 100, and (f) 34 nm, respectively.

3.3. Deformation microstructures

SEM secondary-electron images of deformed pillars with d = 360, 100 and 34 nm are shown in Figs. 5(a), (b), Figs. 5(c),(d), and Figs. 5(e), (f), respectively. These SEM observations were made on a side face (parallel to the loading axis) of pillar specimen along the direction 30° inclined from the loading axis so that the trace of the loading axis is seen vertically. The faint striated contrast noted in the vertical direction of these images is due to surface roughness formed during FIB machining. For pillars with d = 360 and 100 nm, deformation markings are clearly observed to run presumably parallel to traces on {111} slip planes in each of grains, regardless of specimens size. This indicates that the deformation

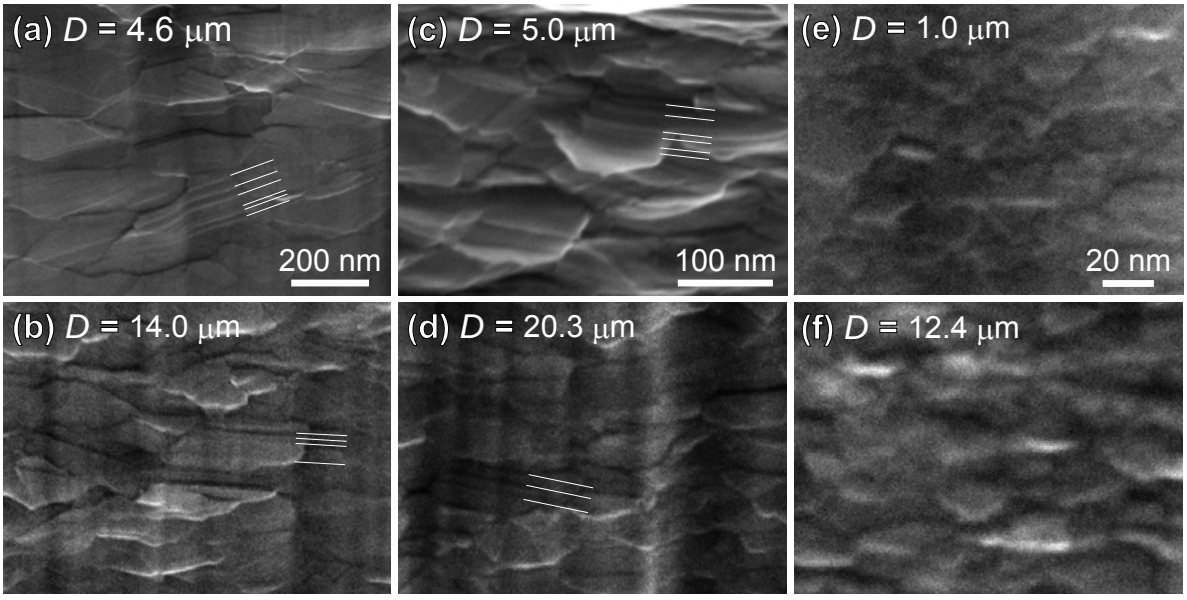

Fig. 5. SEM secondary electron images of a side surface of deformed micropillars with averaged grain sizes d = (a,b) 360, (c,d) 100, and (e,f) 34 nm, respectively. The micropillar size (side length) is written in each image. The micropillar specimens were tilted by 30° from the load axis prior to the surface observation.

mechanisms may not vary significantly depending on whether the ratio of specimen size to grain size (D/d) exceeds the critical value $(D/d)^*$. For pillars with d = 34 nm, on the other hand, deformation markings are hardly observed on the surface of deformed pillars. This was further confirmed by atomic force microscopy. These indicates that the deformation mechanisms for pillars with d = 34 nm are different from those for pillars with d = 360 and 100 nm.

STEM bright-field images of deformation microstructures are shown in Fig. 6 for deformed micropillars with d = 100 and 34 nm. Many dislocations are observed to be introduced both in the surface and inner grains during deformation for pillars with d = 100 nm, regardless of whether the specimen size is smaller (3.3 μm) (Fig. 6(a)) or larger (13.5 μm) (Fig. 6(b)) than the critical size (12.5 μm), below which the yield stress decreases with the decrease in the specimen size. This is consistent with the results of SEM observations that deformation markings presumably parallel to traces on {111} slip planes is observed in each of grains, regardless of specimen size for pillar with d = 360 nm. In contrast, dislocations are hardly observed for deformed pillars with d = 34 nm (Fig. 6(c)), regardless of specimen size as well as position (interior or surface of the specimen). This is also consistent with the results of SEM observations that deformation markings are hardly observed on the surface of deformed pillars d = 34 nm. This is in agreement with the results by Chokshi et al. (Chokshi et al., 1989) that grain size-induced softening occurs below 50 nm for Cu. Although twins (or

stacking faults) are observed in some grains as indicated by arrows in Fig. 6, they may be growth twins but not deformation twins when judged from the density change before and after deformation.

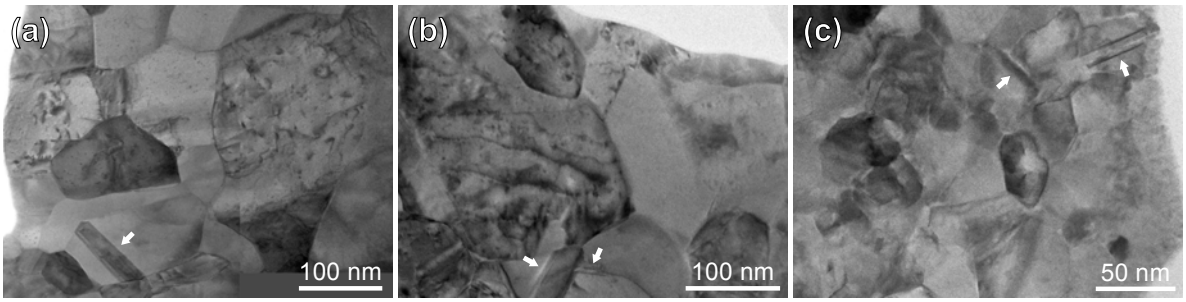

Fig. 6. STEM bright-field images of deformation microstructures for nanocrystalline Cu with d = (a,b) 100, and (c) 34 nm, respectively. The micropillar sizes are (a) 3.3 and (b) 13.5, and (c) 20 μm, respectively.

4. Discussion

4.1. Deformation mechanisms of nanocrystalline Cu

As shown in Fig. 4, although the yield stress significantly decreases as the specimen size is decreased when the specimen size is small (below the critical $(D/d)^*$ values) for pillars with d = 360 and 100 nm, it does not depends on specimen size when the specimen size is sufficiently large for all pillars with d = 360, 100 and 34 nm. Values of bulk yield stress that is independent of specimen size are plotted in Fig. 7 as a function of the inverse square root of grain size for pillars with d = 360, 100 and 34 nm, together with those previously obtained for micrometer-sized Cu (with d = 10−370 μm (Miyazaki and Fujita, 1978; Miyazaki et al., 1979)

and d = 2−24 μm (Yang et al., 2012)). The values of bulk yield stress for pillars with d = 360 and 100 nm increase with the decrease in grain size according to the Hall−Petch relationship (Hall, 1951; Petch, 1953) so that these data points are plotted very close to the line extrapolated from those obtained for micrometer-sized Cu with d = 2−370 μm (Miyazaki and Fujita, 1978; Miyazaki et al., 1979; Yang et al., 2012). The obtained Hall−Petch slope is 0.17 MN/m$^{3/2}$, which is within the range of the slope values so far reported for Cu (0.11-0.35 MN/m$^{3/2}$) (Hommel and Kraft, 2001; Sanders et al., 1997; Vöhringer, 1976). This is consistent with the results of SEM and STEM observations of the deformation structures that dislocation glide within grains is the dominant deformation mechanism for these pillars with d = 360 and 100 nm. The value of bulk yield stress for pillars with d = 34 nm, on the other hand, is smaller

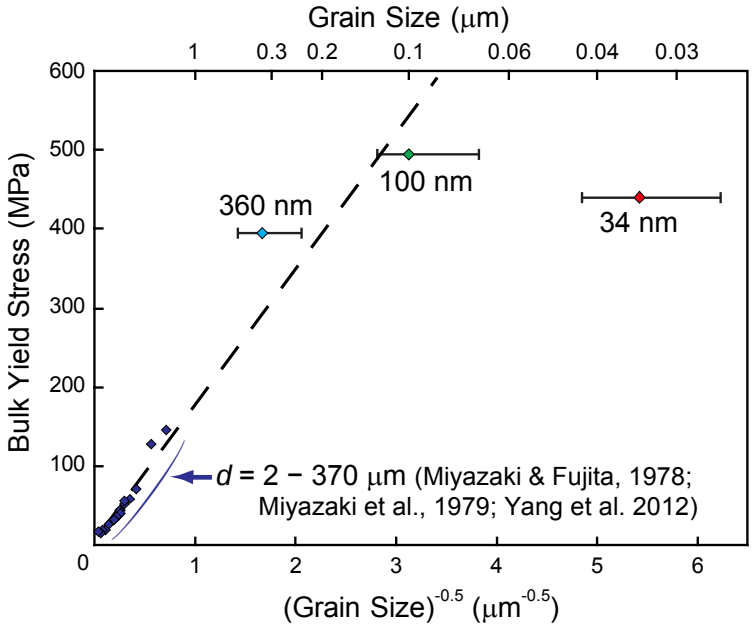

Fig. 7. Values of bulk yield stress plotted as a function of the inverse square root of grain size together with those for coarse-grained Cu polycrystals (Miyazaki and Fujita, 1978; Miyazaki et al., 1979; Yang et al., 2012).

than that for pillars with d = 100 nm, exhibiting the so-called inverse Hall–Petch relationship. The data point for pillars with d = 34 nm is considerably smaller than that expected from the extrapolated Hall–Petch line. This is also consistent with the results of SEM and STEM observations that mechanisms other than dislocation glide within grains is responsible for deformation of pillars with d = 34 nm. This can be further confirmed by the fact that the average size (52 nm) of Frank-Read type dislocation sources simply calculated by the equation of $l = 2\mu b/\sigma_y$ (where μ, b and σ_y stand for the shear modulus, the magnitude of the Burgers vector for perfect dislocations, and the macroscopic yield stress, respectively) with the values of μ = 44 GPa, and b = 0.256 nm (ASM, 1990; Villars, 1997) is larger than the grain size of 34 nm.

Deformation mechanisms that operate in pillars with d = 34 nm may be GB-mediated such as grain rotation (Shan et al., 2004; Wang et al., 2008), GB diffusional creep (Coble creep) (Coble, 1963; Pande and Cooper, 2009) and GB migration (Gianola et al., 2006; Legros et al., 2008; Rupert et al., 2009), in view of the fact that neither deformation markings nor dislocations are observed by SEM and TEM. GB diffusional creep (Coble creep) may be one of the most plausible deformation mechanisms that operate for pillars with d = 34 nm in compression made at a low strain rate (3×10^{-5}–3×10^{-4} s^{-1}) in the present study, since the displacement required for a single grain (1.7×10^{-3} nm/s) is calculated to be comparable to the diffusion distance (3.9×10^{-3} nm/s) in the GBs when calculated with the GB diffusion

coefficient for pure Cu (Kaur et al., 1989) by the equation proposed for the Coble creep (Coble, 1963),

$$\tau \propto \frac{d^3 kT}{\delta D_{gb} \Omega} \dot{\varepsilon} \quad (1)$$

where $\dot{\varepsilon}$ is the strain rate, δ is the effective GB thickness (assumed to be 1 nm), D_{gb} is the self-diffusion coefficient in GBs, Ω is the vacancy volume, k is Boltzmann's constant, and T is absolute temperature (300 K). Indeed, it has been reported that the dominant deformation mechanism of nanocrystalline Ni is the Coble creep at room temperature (Wang et al., 1997) though the creep rate is smaller than 10^{-5} s^{-1} due to the low GB diffusion coefficient for pure Ni (Kaur et al., 1989).

Figure 8 depicts schematically how the bulk yield stress of fcc polycrystals depends on grain size based on the present results. Three distinct deformation mechanisms, dislocation glide, deformation twinning, and GB diffusional (Coble) creep, are considered to operate alternately depending on grain size. For coarse-grained polycrystals, dislocation glide is the predominant deformation mechanism and the bulk yield stress varies linearly with the inverse square root of grain size ($\sim d^{-0.5}$). As the grain size becomes smaller, dislocation glide is still the predominant deformation mechanism. But, deformation becomes much more source-limited, leading to the d^{-1} dependence of bulk yield stress (Asaro et al., 2003; Asaro and Suresh, 2005). As the grain size becomes still smaller, deformation twinning is sometimes reported to be the dominant deformation mechanism accompanied by a similar d^{-1} dependence

of bulk yield stress, although the grain size dependence is not significant when compared to that for source-limited dislocation glide (Asaro and Suresh, 2005; Zhu et al., 2012). Mechanistic model calculation predicts that the transition from dislocation glide to deformation twinning occurs at a grain size of 40−46 nm for Cu (Asaro and Suresh, 2005; Zhu et al., 2012). As the grain size is further reduced, dislocation glide is no longer the predominant deformation mechanism and GB-mediated deformation started to occur. Coble creep dictates the d^3 dependence of bulk yield stress (Coble, 1963), so that the bulk yield stress rapidly decreases with the decrease in grain size in Fig. 8. As is easily recognized from Eq. (1), the bulk yield stress for Coble creep strongly depends on strain rate. When the

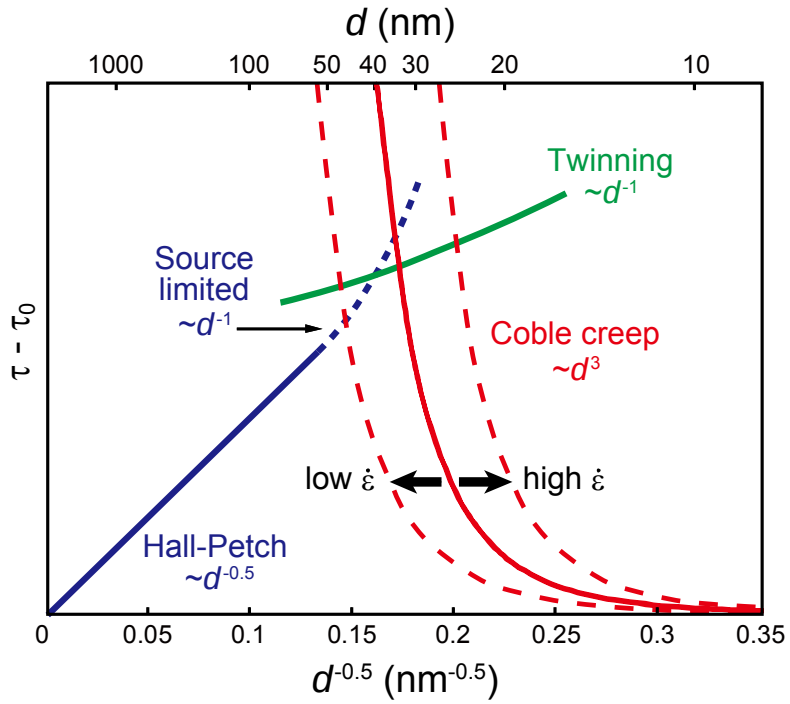

Fig. 8. Grain size dependence of the strengthening component of the critical resolved shear stress (τ - τ_0). Since the stress required for the Coble creep is highly strain-rate sensitive, the τ *vs.* $d^{-0.5}$ curve for the Coble creep slides along the horizontal axis depending on the strain-rate.

strain rate is very high (of the order of 10^{-2} s^{-1}) as in nanoindentation (Jiang et al., 2003; Trelewicz and Schuh, 2007), the curve for Coble creep shifts towards the smaller grain size side, leading to the transition from the normal to inverse Hall−Petch relationships occurring at smaller grain sizes (10-20 nm) (Detor and Schuh, 2007; Erb, 1995; Schuh et al., 2003; Schuh et al., 2002; Trelewicz and Schuh, 2007, 2008). In this case, deformation twinning operates as the dominant deformation mechanism in the lower bound of grain size for the normal Hall−Petch relationship. When the strain rate is very low as in the present micropillar compression tests (3×10^{-5}–3×10^{-4} s^{-1}), on the other hand, the curve for Coble creep shifts towards the larger grain size side with the transition from the normal to inverse Hall−Petch relationships occurring at larger grain sizes, eliminating the grain size regime for the operation of deformation twinning. This is consistent with what is observed in the present study (the transition occurring at grain sizes more than 34 nm), although a decisive conclusion for the absence of deformation twins cannot be drawn until deformation twins are distinguished from growth ones. Indeed, deformation twinning is usually reported to operate when the strain rate is relatively high (~10^{-2} s^{-1}) (Huang et al., 2006; Sriram et al., 2008).

4.2. Grain-size dependence of the critical size ratio (D/d)*

As seen in Fig. 7, the values of bulk yield stress obtained in the present study for pillars with d = 360 and 100 nm are found to obey the Hall−Petch relationship, so that these

data points are plotted very close to the line extrapolated from those obtained for micrometer-sized Cu with d = 2−370 μm (Miyazaki and Fujita, 1978; Miyazaki et al., 1979; Yang et al., 2012). This strongly indicates that plastic deformation for pillars with d = 360 and 100 nm occurs predominantly by dislocation glide within crystalline grains. Significant softening is observed to occur for these pillars with d = 360 and 100 nm when the specimen size is reduced below the critical $(D/d)^*$ values (35 and 85, respectively), although no transition in deformation mechanisms is noted depending on specimen size (dislocation glide is the dominant deformation mechanism for these pillars regardless of the specimen size investigated, as shown in Figs. 6(a) and (b)). The occurrence of the softening without changing the deformation mechanism (being dislocation glide) observed for pillars with d = 360 and 100 nm in the present study is consistent with what is observed for coarse-grained (micrometer-sized) polycrystalline metals (Miyazaki et al., 1979) but not with what is reported for pillars of nanocrystalline Ni and Pt by Greer et al. (Gu et al., 2012; Jang and Greer, 2011), who attributed the softening to the occurrence of the transition in deformation mechanism of surface grains from dislocation-mediated to GB-mediated. In pillars of nanocrystalline Cu with d = 34 nm in which the deformation mechanism is identified to be GB-mediated (Figs. 5(e) and (f), and Fig. 6(c)) in the present study, however, the specimen size-induced softening is no longer observed.

The critical $(D/d)^*$ values, below which the yield stress starts to decrease, are plotted

in Fig. 9 as a function of grain size for pillars with d = 360 and 100 nm, together with those obtained for coarse-grained (micrometer-sized) polycrystalline Cu (Miyazaki et al., 1979) and those obtained for pillars of nanocrystalline Ni and Pt (Gu et al., 2012; Jang and Greer, 2011). For coarse-grained Cu polycrystals, the critical $(D/d)^*$ values tend to increase with the decrease in grain size, allowing the power law scaling with the exponent of -0.413. Interestingly, the values of $(D/d)^*$ obtained in the present study for nanocrystalline Cu pillars with d = 360 and 100 nm obey the same power law scaling for coarse-grained Cu polycrystals, as seen in Fig. 9. This indicates that the specimen size-induced softening extends from micrometer to nanometer scales and confirms again that the softening for these nanocrystalline pillars occurs without a change in the dominant deformation mechanism, but

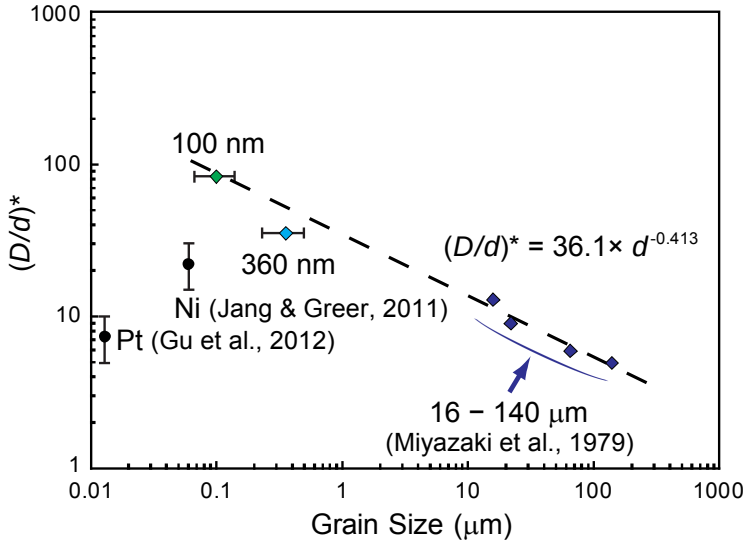

Fig. 9. Critical values of specimen−grain size ratio, $(D/d)^*$, plotted as a function of grain size for the electrodeposited nanocrystalline Cu with d = 360 and 100 nm, coarse grained Cu polycrystals (Miyazaki et al., 1979), 60 nm-grained Ni (Jang and Greer, 2011) and 12 nm-grained Pt (Gu et al., 2012).

with the dominant deformation mechanism being dislocation glide in crystalline grains, as in the case of coarse-grained Cu polycrystals.

The specimen size-induced softening is long known to occur in coarse-grained (micrometer-sized) polycrystals when the ratio of specimen size to grain size is smaller than the critical value, $(t/d)^*$ or $(D/d)^*$ (Armstrong, 1961; Miyazaki et al., 1979; Pell-Walpole, 1943; Thompson, 1974; Thompson et al., 1973), and the critical value, below which the yield stress starts to decrease, generally increases with the decrease in grain size for a given material and with the decrease in stacking fault energy (Miyazaki and Fujita, 1978; Miyazaki et al., 1979). One of the several different explanations for this is as follows. For polycrystals, any grain is constrained to deformation by surrounding grains, because strain continuity must be maintained at the GBs. In order to maintain strain continuity at the GBs, geometrically necessary (GN) dislocations (termed by Ashby (Ashby, 1970)) must be generated generally in the form of multiple slip, in addition to statically stored dislocations. The probability to find out the source to generate GN dislocations in multiple slip is considered to play a role in determining the critical $(D/d)^*$ value, since it determines how many neighboring grains are constrained simultaneously to deformation. Then, it is naturally expected that the probability to find out the source to generate GN dislocations decrease with the decrease in grain size, leading to the higher critical $(D/d)^*$ value, as experimentally observed.

The critical $(D/d)^*$ values for nanocrystalline Cu pillars with d = 360 and 100 nm (35

and 85) are much larger than those reported for coarse grained Cu polycrstals (5−13 for d = 16−140 μm (Miyazaki et al., 1979) and 2 for d = 2−24 μm (Yang et al., 2012)). This may be explained in line with what is described above for coarse-grained polycrystals, since the dominant deformation mechanism stays dislocation glide. These critical (D/d)* values determined for nanocrystalline Cu pillars in the present study are also considerably larger than those determined for 60 nm-grained Ni pillars (15−30) (Jang and Greer, 2011) and 12 nm-grained Pt pillars (5−10) (Gu et al., 2012). Since the values of stacking fault energy for Ni (125−250 mJ/m^2) (Gallagher, 1970; Hirth and Lothe, 1982) and Pt (322 mJ/m^2) (Hirth and Lothe, 1982) are considerably larger than that for Cu (45−55 mJ/m^2) (Gallagher, 1970; Hirth and Lothe, 1982), cross-slip occurs more easily in Ni and Pt, making the generation of GN dislocations more easily. Thus, the smaller (D/d)* values are obtained for Ni and Pt, as experimentally observed in coarse-grained polycrystals (Miyazaki and Fujita, 1978; Miyazaki et al., 1979; Yang et al., 2012).

Conclusions

(1) The yield stress for nanocrystalline Cu pillars with d = 360 and 100 nm does not depend on specimen size, exhibiting essentially the same values as their respective bulk specimen when the specimen size is large, while when the specimen size is small, the yield stress significantly decreases as the specimen size is decreased. In contrast, the yield stress for

nanocrystalline Cu pillars with d = 34 nm does not depend much on specimen size, exhibiting the bulk yield stress value for all specimen sizes investigated.

(2) The value of bulk yield stress for pillars with d = 34 nm is smaller than those for pillars with d = 360 and 100 nm, indicating the occurrence of grain-size induced softening, in agreement with the previous results by Chokshi et al. (Chokshi et al., 1989) that grain size-induced softening occurs below 50 nm for Cu.

(3) While dislocation glide within crystalline grains is the dominant deformation mechanism for nanocrystalline Cu pillars with d = 360 and 100 nm, GB diffusional creep is dominant for pillars with d = 34 nm.

(4) The critical $(D/d)^*$ values, below which the yield stress starts to decrease, determined for nanocrystalline Cu pillars with d = 360 and 100 nm (35 and 85) increase with the decrease in grain size so as to conform to the same power law scaling obtained for coarse-grained Cu polycrystals, indicating that the specimen size-induced softening extends from micrometer to nanometer scales as far as the dominant deformation mechanism is dislocation glide. The considerably large critical $(D/d)^*$ values determined for nanocrystalline Cu pillars with d = 360 and 100 nm are explained in terms of the probability to find out the source to generate GN dislocations in multiple slip, in line with what has been described for coarse-grained polycrystals.

Acknowledgements

This work was supported by JSPS KAKENHI grant numbers 24246113 and 25709066, and the Elements Strategy Initiative for Structural Materials (ESISM) from the Ministry of Education, Culture, Sports, Science and Technology (MEXT) of Japan, and in part by Advanced Low Carbon Technology Research and Development Program (ALCA) from the Japan Science and Technology Agency (JST).

References

- Arioka, T., Hori, M., Toki, T., Yakawa, A., Morikawa, M., 2001. Growth mechanism of dross particles in molten Zn baths, in: Lamberights, M. (Ed.), 5th International Conference on Zinc and Zinc Alloy Coated Steel Sheet. Verlag Stahleisen, Brussels, Belgium, pp. 393-400.
- Armstrong, R.W., 1961. On Size Effects in Polycrystal Plasticity. J. Mech. Phys. Solids 9, 196-199.
- Asaro, R.J., Krysl, P., Kad, B., 2003. Deformation mechanism transitions in nanoscale fcc metals. Philos. Mag. Lett. 83, 733-743.
- Asaro, R.J., Suresh, S., 2005. Mechanistic models for the activation volume and rate sensitivity in metals with nanocrystalline grains and nano-scale twins. Acta Mater. 53, 3369-3382.
- Ashby, M.F., 1970. Deformation of Plastically Non-Homogeneous Materials. Philos. Mag. 21, 399-&.
- ASM, 1990. Properties and Selection : Nonferrous Alloys and Special-Purpose Materials, 10th ed. ASM International, Materials Park, OH.
- Chen, J., Lu, L., Lu, K., 2006. Hardness and strain rate sensitivity of nanocrystalline Cu. Scripta Mater. 54, 1913-1918.
- Chen, X.X., Ngan, A.H.W., 2011. Specimen size and grain size effects on tensile strength of Ag microwires. Scripta Mater. 64, 717-720.
- Chokshi, A.H., Rosen, A., Karch, J., Gleiter, H., 1989. On the Validity of the Hall-Petch Relationship in Nanocrystalline Materials. Scripta Metall. 23, 1679-1683.
- Coble, R.L., 1963. A Model for Boundary Diffusion Controlled Creep in Polycrystalline Materials. J. Appl. Phys. 34, 1679-&.
- Detor, A.J., Schuh, C.A., 2007. Tailoring and patterning the grain size of nanocrystalline alloys. Acta Mater. 55, 371-379.
- Erb, U., 1995. Electrodeposited nanocrystals: Synthesis, properties and industrial applications. Nanostruct. Mater. 6, 533-538.
- Gallagher, P.C.J., 1970. Influence of Alloying, Temperature, and Related Effects on Stacking Fault Energy. Metall. Trans. 1, 2429-&.
- Gianola, D.S., Van Petegem, S., Legros, M., Brandstetter, S., Van Swygenhoven, H., Hemker, K.J., 2006. Stress-assisted discontinuous grain growth and its effect on the deformation behavior of nanocrystalline aluminum thin films. Acta Mater. 54, 2253-2263.
- Greer, J.R., De Hosson, J.T.M., 2011. Plasticity in small-sized metallic systems: Intrinsic

versus extrinsic size effect. Prog. Mater Sci. 56, 654-724.
- Greer, J.R., Nix, W.D., 2006. Nanoscale gold pillars strengthened through dislocation starvation. Phys. Rev. B 73, 245410.
- Greer, J.R., Oliver, W.C., Nix, W.D., 2005. Size dependence of mechanical properties of gold at the micron scale in the absence of strain gradients. Acta Mater. 53, 1821-1830.
- Gu, X.W., Loynachan, C.N., Wu, Z.X., Zhang, Y.W., Srolovitz, D.J., Greer, J.R., 2012. Size-Dependent Deformation of Nanocrystalline Pt Nanopillars. Nano Lett. 12, 6385-6392.
- Hall, E.O., 1951. The Deformation and Ageing of Mild Steel .3. Discussion of Results. Proc. Phys. Soc. 64, 747-753.
- Hirth, J.P., Lothe, J.L., 1982. Theory of Dislocations. Wiley, New York.
- Hommel, M., Kraft, O., 2001. Deformation behavior of thin copper films on deformable substrates. Acta Mater. 49, 3935-3947.
- Huang, C.X., Wang, K., Wu, S.D., Zhang, Z.F., Li, G.Y., Li, S., 2006. Deformation twinning in polycrystalline copper at room temperature and low strain rate. Acta Mater. 54, 655-665.
- Hug, E., Keller, C., 2010. Intrinsic Effects due to the Reduction of Thickness on the Mechanical Behavior of Nickel Polycrystals. Metall. Mater. Trans. A 41A, 2498-2506.
- Jang, D.C., Greer, J.R., 2011. Size-induced weakening and grain boundary-assisted deformation in 60 nm grained Ni nanopillars. Scripta Mater. 64, 77-80.
- Janssen, P.J.M., de Keijser, T.H., Geers, M.G.D., 2006. An experimental assessment of grain size effects in the uniaxial straining of thin Al sheet with a few grains across the thickness. Mater. Sci. Eng., A 419, 238-248.
- Jiang, W.H., Pinkerton, F.E., Atzmon, M., 2003. Effect of strain rate on the formation of nanocrystallites in an Al-based amorphous alloy during nanoindentation. J. Appl. Phys. 93, 9287-9290.
- Kaur, I., Gust, W., Kozma, L., 1989. Handbook of grain and interphase boundary diffusion data. Ziegler Press, Stuttgart.
- Keller, C., Hug, E., Feaugas, X., 2011. Microstructural size effects on mechanical properties of high purity nickel. Int. J. Plast. 27, 635-654.
- Knapp, J.A., Follstaedt, D.M., 2004. Hall-Petch relationship in pulsed-laser deposited nickel films. J. Mater. Res. 19, 218-227.
- Kraft, O., Gruber, P.A., Monig, R., Weygand, D., 2010. Plasticity in Confined Dimensions. Annu. Rev. Mater. Res. 40, 293-317.
- Legros, M., Gianola, D.S., Hemker, K.J., 2008. In situ TEM observations of fast

grain-boundary motion in stressed nanocrystalline aluminum films. Acta Mater. 56, 3380-3393.

- Machalett, F., Edinger, K., Melngailis, J., Diegel, M., Steenbeck, K., Steinbeiss, E., 2000. Direct patterning of gold oxide thin films by focused ion-beam irradiation. Appl. Phys. A 71, 331-335.
- Miyazaki, S., Fujita, H., 1978. Effects of Grain-Size and Specimen Thickness on Mechanical-Properties of Polycrystalline Copper and Copper-Aluminum Alloy. Trans. Japan Inst. Met. 19, 439-444.
- Miyazaki, S., Shibata, K., Fujita, H., 1979. Effect of Specimen Thickness on Mechanical-Properties of Polycrystalline Aggregates with Various Grain Sizes. Acta Metall. 27, 855-862.
- Overwijk, M.H.F., Vandenheuvel, F.C., Bullelieuwma, C.W.T., 1993. Novel Scheme for the Preparation of Transmission Electron-Microscopy Specimens with a Focused Ion-Beam. J. Vac. Sci. Technol., B 11, 2021-2024.
- Pande, C.S., Cooper, K.P., 2009. Nanomechanics of Hall-Petch relationship in nanocrystalline materials. Prog. Mater Sci. 54, 689-706.
- Pell-Walpole, W.T., 1943. Tide effect of grain-size on the tensile strength of tin and tin alloys. J. Inst. Metal 69, 131-146.
- Petch, N.J., 1953. The Cleavage Strength of Polycrystals. J. Iron Steel Inst. 174, 25-28.
- Rupert, T.J., Gianola, D.S., Gan, Y., Hemker, K.J., 2009. Experimental Observations of Stress-Driven Grain Boundary Migration. Science 326, 1686-1690.
- Sanders, P.G., Eastman, J.A., Weertman, J.R., 1997. Elastic and tensile behavior of nanocrystalline copper and palladium. Acta Mater. 45, 4019-4025.
- Schuh, C.A., Nieh, T.G., Iwasaki, H., 2003. The effect of solid solution W additions on the mechanical properties of nanocrystalline Ni. Acta Mater. 51, 431-443.
- Schuh, C.A., Nieh, T.G., Yamasaki, T., 2002. Hall-Petch breakdown manifested in abrasive wear resistance of nanocrystalline nickel. Scripta Mater. 46, 735-740.
- Shan, Z.W., Stach, E.A., Wiezorek, J.M.K., Knapp, J.A., Follstaedt, D.M., Mao, S.X., 2004. Grain boundary-mediated plasticity in nanocrystalline nickel. Science 305, 654-657.
- Sriram, V., Yang, J.M., Ye, J., Minor, A.M., 2008. Determining the stress required for deformation twinning in nanocrystalline and ultrafine-grained copper. JOM 60, 66-70.
- Thompson, A.W., 1974. Use of Nonpolycrystal Specimens in Mechanical-Behavior Tests. Scripta Metall. 8, 145-147.

- Thompson, A.W., Baskes, M.I., Flanagan, W.F., 1973. Dependence of Polycrystal Work-Hardening on Grain-Size. Acta Metall. 21, 1017-1028.
- Trelewicz, J.R., Schuh, C.A., 2007. The Hall-Petch breakdown in nanocrystalline metals: A crossover to glass-like deformation. Acta Mater. 55, 5948-5958.
- Trelewicz, J.R., Schuh, C.A., 2008. The Hall-Petch breakdown at high strain rates: Optimizing nanocrystalline grain size for impact applications. Appl. Phys. Lett. 93, 171916.
- Uchic, M.D., Shade, P.A., Dimiduk, D.M., 2009. Plasticity of micrometer-scale single crystals in compression. Annu. Rev. Mater. Res. 39, 361-386.
- Van Swygenhoven, H., Derlet, P.A., 2001. Grain-boundary sliding in nanocrystalline fcc metals. Phys. Rev. B 64.
- Villars, P., 1997. Pearson's Handbook: Crystallographic Data for Intermetallic Phases. ASM International, Amsterdam.
- Vöhringer, O., 1976. Flow-Stress for Twinning of Alpha-Copper-Alloys. Z. Metallkd. 67, 518-524.
- Wang, N., Wang, Z.R., Aust, K.T., Erb, U., 1997. Room temperature creep behavior of nanocrystalline nickel produced by an electrodeposition technique. Mater. Sci. Eng., A 237, 150-158.
- Wang, Y.B., Li, B.Q., Sui, M.L., Mao, S.X., 2008. Deformation-induced grain rotation and growth in nanocrystalline Ni. Appl. Phys. Lett. 92.
- Warthi, N., Ghosh, P., Chokshi, A.H., 2013. Approaching theoretical strengths by synergistic internal and external size refinement. Scripta Mater. 68, 225-228.
- Yang, B., Motz, C., Rester, M., Dehm, G., 2012. Yield stress influenced by the ratio of wire diameter to grain size - a competition between the effects of specimen microstructure and dimension in micro-sized polycrystalline copper wires. Philos. Mag. 92, 3243-3256.
- Zhu, Y.T., Liao, X.Z., Wu, X.L., 2012. Deformation twinning in nanocrystalline materials. Prog. Mater Sci. 57, 1-62.

Figure Legends

Fig. 1. (a-c) Bright-field TEM images, and (d-f) selected area diffraction patterns for the nanocrystalline Cu electrodeposited with the thiourea concentration of (a,d) 0, (b,e) 1.2, and (c,f) 67 mg/L, respectively.

Fig. 2. Grain size distributions for the nanocrystalline Cu electrodeposited with the thiourea concentration of (a) 0, (b) 1.2, and (c) 67 mg/L, respectively. The curves and dotted lines are lognormal regression curves and arithmetic mean grain sizes, respectively.

Fig. 3. XRD patterns obtained for electrodeposited Cu films with average grain size of 360, 100, and 34nm. Calculated patterns for randomly oriented fcc Cu, CuO, Cu_2O and CuS are also shown below the experimental ones.

Fig. 4. Representative compression stress−strain curves for pillars of various sizes fabricated from the electrodeposited films with d = (a) 360, (b) 100, and (c) 34 nm, respectively. Values of yield stress plotted as a function of the specimen size (side length, D) for d = (d) 360, (e) 100, and (f) 34 nm, respectively.

Fig. 5. SEM secondary electron images of a side surface of deformed micropillars with averaged grain sizes d = (a,b) 360, (c,d) 100, and (e,f) 34 nm, respectively. The micropillar size (side length) is written in each image. The micropillar specimens were tilted by 30° from the load axis prior to the surface observation.

Fig. 6. STEM bright-field images of deformation microstructures for nanocrystalline Cu with d = (a,b) 100, and (c) 34 nm, respectively. The micropillar sizes are (a) 3.3 and (b) 13.5, and (c) 20 μm, respectively.

Fig. 7. Values of bulk yield stress plotted as a function of the inverse square root of grain size together with those for coarse-grained Cu polycrystals (Miyazaki and Fujita, 1978; Miyazaki et al., 1979; Yang et al., 2012).

Fig. 8. Grain size dependence of the strengthening component of the critical resolved shear stress (τ - τ_0). Since the stress required for the Coble creep is highly strain-rate sensitive, the τ *vs.* $d^{-0.5}$ curve for the Coble creep slides along the horizontal axis depending on the strain-rate.

Fig. 9. Critical values of specimen−grain size ratio, (D/d)*, plotted as a function of grain size for the electrodeposited nanocrystalline Cu with d = 360 and 100 nm, coarse grained Cu polycrystals (Miyazaki et al., 1979), 60 nm-grained Ni (Jang and Greer, 2011) and 12 nm-grained Pt (Gu et al., 2012).